

THE MOLECULAR ENVELOPE AROUND THE RED SUPERGIANT VY CMA

MULLER S., DINH-V-TRUNG, LIM J., HIRANO N.

Academia Sinica Institute of Astronomy and Astrophysics (ASIAA), P.O. Box 23-141, Taipei, 106 Taiwan

MUTHU C.

Aryabhata Research Institute of Observational Sciences (ARIES), Manora Peak, Nainital 263129, India

AND

KWOK S.

Department of Physics, Faculty of Science, University of Hong Kong

Draft version October 17, 2018

ABSTRACT

We present millimeter interferometric observations of the molecular envelope around the red supergiant VY CMA with the SubMillimeter Array (SMA)¹. The high angular resolution ($< 2''$) allows us to derive the structure of the envelope as observed in the 1.3 mm continuum, ¹²CO(2-1), ¹³CO(2-1) and SO(6₅-5₄) lines emission. The circumstellar envelope is resolved into three components: a dense, compact and dusty central component, embedded in a more diffuse and extended envelope plus a high velocity component. We construct a simple model, consisting of a spherically symmetric slowly expanding envelope and bipolar outflows with a wide opening angle ($\sim 120^\circ$) viewed close to the line of sight ($i = 15^\circ$). Our model can explain the main features of the SMA data and previous single-dish CO multi-line observations. An episode of enhanced mass loss along the bipolar direction is inferred from our modelling. The SMA data provide a better understanding of the complicated morphology seen in the optical/IR high resolution observations.

Subject headings: circumstellar matter – supergiants – stars: individual (VY Canis Majoris) – radio lines: stars

1. INTRODUCTION

The terminal stage in the evolution of massive stars ($M > 10 M_\odot$) is characterized by very short timescales ($\sim 10^4$ yr) and drastic changes in their immediate circumstellar environment. In the red supergiant phase, periods of large mass loss release a thick circumstellar envelope of molecular gas and dust. Understanding the mass loss process from red supergiants is extremely important in that it will eventually govern their evolution as well as the structure of their surrounding envelope. In a galactic context, supergiants contribute to the enrichment of the interstellar medium in dust and heavy elements and participate to the global galactic chemical evolution.

VY Canis Majoris (VY CMA) is one of the brightest known red supergiants. Its distance has long been debated (Herbig 1970; Lada & Reid 1978), but there is now a consensus on a value of 1.5 kpc, consistent with the velocity and proper motions of H₂O masers (Richards et al. 1998). The stellar luminosity is estimated to $\sim 2 \cdot 10^5 L_\odot$ (Monnier et al. 1999). The stellar mass is thought to be $\geq 15 M_\odot$. The basic properties of VY CMA are summarized in Table 1.

VY CMA is characterized by an apparent very high mass loss rate, of order $2 - 4 \cdot 10^{-4} M_\odot/\text{yr}$ (see *e.g.* Bowers et al. 1983; Danchi et al. 1994; Stanek et al.

1995; Harwit et al. 2001), which produced a very thick circumstellar envelope of dust and molecules, which almost completely obscures the central star. The optical/infrared morphology of the nebulosity around VY CMA is very complex, showing arcs, filaments, bright knots in a very complicated arrangement (Smith et al. 2001; Monnier et al. 1999). Long slit spectroscopy (Smith 2004; Humphreys et al. 2005) reveals a very complex kinematics with evidence for localized and episodic mass loss events. Humphreys et al. (2005) showed that the prominent arcs are expanding relative to the star and represent discrete ejection events. The ejection dates are ranging from 200 to 1000 years ago and state that VY CMA has had a period of major activity during the past 1000 years. These works however rely on scattered lights which may reflect only the illuminated part of the nebula and the origin of the features seen in the optical and near infrared images is very uncertain.

We note that in a recent paper, Decin et al. (2006) propose a theoretical model, based on a spherically symmetric envelope, that requires time varying mass-loss rates to reproduce previous single-dish CO multi-line spectra. The high angular resolution view offered by the SubMillimeter Array (SMA) now provides new constraints on the structure and kinematics of the circumstellar molecular envelope of this peculiar object. In this paper, we present our SMA observations and discuss about the morphology and kinematics of the molecular envelope around VY CMA. We propose a simple model to explain our data and compare with observations at other wavelengths.

Electronic address: muller, trung, jlim, hirano@asiaa.sinica.edu.tw
Electronic address: muthu@aries.ernet.in
Electronic address: sunkwok@hkucc.hku.hk

¹The Submillimeter Array is a joint project between the Smithsonian Astrophysical Observatory and the Academia Sinica Institute of Astronomy and Astrophysics and is funded by the Smithsonian Institution and the Academia Sinica.

2. OBSERVATIONS

We obtained 1.3 mm interferometric observations of VY CMa with the Submillimeter Array (SMA, Ho et al. 2004), which consists of eight 6 m antennas, located on top of the Mauna Kea, Hawaii. The phase reference of the array was set to R.A. = $07^{\text{h}}22^{\text{m}}58^{\text{s}}.328$ and Dec. = $-25^{\circ}46'03''.19$.

VY CMa was observed at 2 different epochs and with 2 different configurations. The first observation was carried out on 2004 July 31st, with 7 antennas in a compact configuration, including projected baselines from 8 to 99 m. The system temperatures at 1 mm were between 100 and 200 K for the different antennas. In order to improve the angular resolution, a second track was observed on 2005 January 19th, with 7 antennas in an extended configuration. The projected baselines ranged from 18 to 192 m. The system temperatures were between 200 and 400 K. The bandpass was calibrated using Uranus and/or Jupiter, while Callisto set the flux calibration. The nearby quasars 0607–157 and 0730–116 were regularly observed for the gain calibration. After calibration, the visibilities from both tracks have been combined together. The data reduction and calibration were done under MIR/IDL. Imaging and data analysis were entirely processed under GILDAS¹.

The heterodyne receivers were tuned to allow multi-line observations including the $^{12}\text{CO}(2-1)$ line in the upper side band (USB) and the $^{13}\text{CO}(2-1)$ and $\text{SO}(6_5-5_4)$ lines in the lower side band (LSB). The SMA correlator bandwidth is 2 GHz wide for each sidebands, which are separated by 10 GHz. The instrumental spectral resolution was 0.8125 MHz, but we smoothed it to 3.25 MHz (*i.e.* $\sim 4 \text{ km s}^{-1}$) for the $^{12}\text{CO}(2-1)$ and $\text{SO}(6_5-5_4)$ lines and to 8.125 MHz (*i.e.* $\sim 11 \text{ km s}^{-1}$) in the case of $^{13}\text{CO}(2-1)$.

We obtained the map of the 1.3 mm (225 GHz) continuum emission by averaging the line-free channels from both LSB and USB, resulting in a total bandwidth of 3 GHz. To maximize the angular resolution, we applied uniform weighting to the continuum visibilities, leading to a synthesized beam size of $1.38'' \times 1.23''$ (PA = 169°). We estimate a rms noise level of 8 mJy/beam in this continuum map.

The channel maps of the $^{12}\text{CO}(2-1)$ and $\text{SO}(6_5-5_4)$ line emission were obtained using natural weighting and gaussian tapering with a full width at half maximum (FWHM) of 130 m, making a compromise between brightness sensitivity and angular resolution. The $^{13}\text{CO}(2-1)$ map was derived using a taper distance of 80 m to increase the signal-to-noise ratio. The resulting synthesized beam sizes and 1σ noise levels are reported in Table 2. The continuum visibilities were subtracted before imaging. All the maps were deconvolved with a standard CLEAN/CLARK algorithm.

At 230 GHz, the FWHM of the 6 m SMA antennas primary beam is $54''$. The shortest projected baseline being 8 m, we may lose informations on structures larger than $40''$. Nevertheless, the resulting coverage of the uv-plane is rather scarce until 18 m. We may therefore also miss part of the emission associated with structures larger than $18''$, although we show in §3.2.2 from the

comparison of the $^{12}\text{CO}(2-1)$ SMA and single dish data, that the missing flux is limited to less than 20 %.

3. RESULTS

3.1. 1.3 mm continuum emission

Lipsy et al. (2005) observed VY CMa at centimeter wavelengths using the VLA. They do not resolve the source at an angular resolution of $\sim 1''$ at 1.3 cm. They also present Keck mid-infrared imaging and show that the dust emission is elongated in the south-west direction (PA = 227°) with FWHM $\sim 0.4''$ and $0.3''$ at 11.7 and $17.9 \mu\text{m}$ respectively. From diffraction-limited speckle interferometry, Wittkowski et al. (1998) measure a dust shell size of $138 \times 205 \text{ mas}$ ($2.17 \mu\text{m}$), $80 \times 116 \text{ mas}$ ($1.28 \mu\text{m}$) and $67 \times 83 \text{ mas}$ ($0.8 \mu\text{m}$) with roughly a north-south elongation. Thus, at near-IR wavelengths, the size of the dust-emitting region decreases towards shorter wavelengths, progressively tracing warmer dust close to the star.

As seen from Fig.1, the continuum emission is not resolved by our synthesized beam ($\sim 1.4''$). The continuum visibilities are well fitted by a point source of $288 \pm 25 \text{ mJy}$ (with 3σ rms), located at a position $+0.15'' \pm 0.01''$ to the east and $-0.05'' \pm 0.01''$ to the south, relatively to the phase center. Our measurement of the flux density is consistent with the value of $270 \pm 40 \text{ mJy}$ from previous SMA observations at 215 GHz (Shinnaga et al. 2004) but differs from the previous bolometric values of $630 \pm 65 \text{ mJy}$ obtained with the JCMT (Knapp et al. 1993) and $378 \pm 20 \text{ mJy}$ with the SEST (Walmsley 1991). Part of the difference could be explained by contamination from line emission in the bolometric observations. We note, however, that even the $^{12}\text{CO}(2-1)$ line, presumably the strongest in this frequency band, contributes only for about 2% and 7% of the total flux density measurements with the JCMT and SEST, respectively. On the other hand, we cannot exclude the presence of an extended low surface brightness emission that could have been missed in our observations. Independent checks of the continuum flux density in the upper and lower side bands give consistent values within 10%, implying that our measurements are not severely contaminated by weak line emission.

Because the continuum emission is of order of $\sim 1 \text{ mJy}$ in the centimeter wavelengths (Lipsy et al. 2005) and given that the contribution of the central star (black body emission) amounts for $S_* \sim 10 \text{ mJy}$, *i.e.* is negligible with respect to the total 1.3 mm continuum emission S_ν , this latter should arise almost completely from dust thermal emission. Under the Rayleigh-Jeans approximation and if the dust emission is optically thin, we can estimate the dust mass M_d within our $1.4''$ beam, according to:

$$M_d = \frac{2c^2 D^2 a_g \rho_g (S_\nu - S_*)}{3Q_\nu k T_d \nu^2} \quad (1)$$

where D is the distance to the source, ρ_g and a_g are the mass density and radius of the dust grains, Q_ν is the grain emissivity and T_d the average temperature of the dust envelope. We assume typical values for oxygen rich stars, $a_g = 0.2 \mu\text{m}$, $\rho_g = 3.5 \text{ g.cm}^{-3}$, $Q_\nu = 5.65 \cdot 10^{-4} (\nu / 274.6 \text{ GHz})$, following Knapp et al. (1993). The ratio of IR fluxes indicates a temperature $T_d \sim 250 \text{ K}$ in the dust

¹ <http://www.iram.fr/IRAMFR/GILDAS/>

shell (Lipscy et al. 2005). Accordingly, we derive a dust mass of $1.5 \cdot 10^{-3} M_{\odot}$, close to the value $M_d = 1.3 \cdot 10^{-3} M_{\odot}$ given by Lipscy et al. (2005). Assuming that the dust is uniformly distributed within a radius comparable to our synthesized beam (upper limit of $1.4''$), the optical depth towards the central star would be $\tau_{1.3mm} \sim 0.01$.

Furthermore, assuming an expanding velocity $V_{\text{exp}} = 15 \text{ km s}^{-1}$ (similar to the escape velocity of $\sim 20 \text{ km s}^{-1}$ at the dust formation radius, see also §4) leads to an age of order of 300 years. The average mass loss rate over this timescale is $4.7 \cdot 10^{-4} M_{\odot}/\text{yr}$, assuming an isotropic mass loss and a dust-to-gas ratio of 100. This value is slightly higher than previous measurements for VY CMA (see *e.g.* Danchi et al. 1994; Harwit et al. 2001) and comparable to mass loss rates estimated for other supergiants (Netzer & Knapp 1987). Smith et al. (2001) and Humphreys et al. (2005) showed that localized and short-term ejection events in VY CMA could in fact reach $10^{-3} M_{\odot}/\text{yr}$.

On the other hand, as pointed out by the referee, there is a possibility that the continuum dust emission originates from a circumstellar disk, as advocated earlier by Bowers et al. (1983) and Richards et al. (1998) from observations of OH and H₂O maser emissions. However, the angular resolution of our current data is not enough to constrain this possibility.

3.2. Molecular line emission

3.2.1. Description of the molecular line emission

The ¹²CO(2-1) emission (Fig.2) extends to $\sim 7''$ around the central star and is detected over a (LSR) velocity range -25 to 70 km s^{-1} . There are three distinct emission peaks in the channel maps: a first one at a velocity of about -5 km s^{-1} with an offset of $1''$ to the east, a second one close to the systemic velocity of VY CMA ($V_{\text{SYS}} \sim 22 \text{ km s}^{-1}$), centered on the stellar position and a third one around $+45 \text{ km s}^{-1}$ with an offset of $1''$ to the west. The line emission is stronger in the western redshifted part of the nebula, where it reaches $\sim 5 \text{ Jy/beam}$. The velocity channels around the systemic velocity of VY CMA ($12 < V_{\text{LSR}} < 33 \text{ km s}^{-1}$) show a north-south elongated structure of roughly $5'' \times 3''$, embedded in a more diffuse envelope. A second weak peak is seen $3''$ to the west.

Our ¹³CO(2-1) channel maps (Fig.3), although of low signal-to-noise, present globally the same features as seen in ¹²CO(2-1). The two peaks are well detected at velocities ~ -5 and $+50 \text{ km s}^{-1}$, and separated by $\sim 2''$. The emission around the systemic velocity is weakly detected. The channel maps of the SO(6₅-5₄) emission (Fig.4) also show the same features as that of the ¹²CO(2-1). The integrated intensity maps for the three species are presented in Fig.5.

The morphology and kinematics of the ¹²CO(2-1) emission around VY CMA do not reproduce those of a typical spherical expanding shell. We interpret the east and west offset bright peaks, with high velocity relatively to the systemic velocity, as the signature of a east-west bipolar outflow. Shinnaga et al. (2003) already suggested the presence of a bipolar outflow around VY CMA from the butterfly like shape of the SiO(1-0) emission. The idea was further supported by SiO masers linear polarization measurements (Shinnaga et al. 2004), which result

in a mean polarization position angle of 72° , in the axis of the SiO bipolar structure. Previous observations of OH (Bowers et al. 1983, 1993) and H₂O (Richards et al. 1998) masers also show some elongation in a similar direction with position angles of 50° and 60° , respectively. However, the maser emission is clumpy and might not trace the complete geometry of the outflow.

In addition, the 1.3 mm continuum and CO emission around the systemic velocity indicate the presence of a central dense component. The position-velocity diagrams (Fig.6), along the east-west and north-south directions, *i.e.* along and perpendicular to the outflow axis, support our interpretation. Along the east-west direction, the high velocity bipolar outflow and the slowly expanding shell appear clearly as two distinct kinematic components. The bipolar outflow emission shows a point symmetry relative to the stellar position. It extends to roughly $5''$ from the star and has a velocity up to 45 km s^{-1} with respect to the systemic velocity. This corresponds to a timescale of about 800 yr, comparable to the past period of strong mass loss activity (Humphreys et al. 2005; Decin et al. 2006). The slowly expanding envelope can be seen out to a radius of roughly $5''$. Given an expansion velocity of 15 km s^{-1} (see §4), the corresponding timescale is 2400 yr. The overall features are similar in the ¹²CO(2-1) and SO(6₅-5₄) position-velocity diagrams, indicating that they arise from the same regions.

3.2.2. Comparison with single dish spectra

We present in Fig.7 the spectra of the ¹²CO(2-1), ¹³CO(2-1) and SO(6₅-5₄) lines, taken at the central position and convolved to a beam size of FWHM $19''.7$, equal to the JCMT beam at 230 GHz. The ¹²CO(2-1) line profile obtained from our interferometric data can then be directly compared to the single-dish ¹²CO(2-1) spectrum (Kemper et al. 2003) at the same angular resolution. The ¹²CO(2-1) SMA spectrum shows three peaks at $V_{\text{LSR}} \sim -5, 20$ and 45 km s^{-1} , similar with the JCMT spectrum. The high velocity channels ($V_{\text{LSR}} < 5$ and $> 35 \text{ km s}^{-1}$) reach the same brightness temperature as the single-dish observations, indicating that the interferometer recovered all of the emission for these velocities. Close to the systemic velocity of VY CMA, *i.e.* for $5 < V_{\text{LSR}} < 30 \text{ km s}^{-1}$, there is a small difference between the two profiles, although less than $\sim 20\%$ of the emission is lost by the interferometer. We estimate the integrated intensity of the ¹²CO(2-1) line to 65 K km s^{-1} , comparable to the value of $66 \pm 7 \text{ K km s}^{-1}$ reported by Kemper et al. (2003). The integrated intensities of the ¹³CO(2-1) and SO(6₅-5₄) lines are estimated to 4 K km s^{-1} and 28 K km s^{-1} , respectively. The 3σ rms uncertainty is $\sim 1 \text{ K km s}^{-1}$.

3.2.3. SO emission

While carbon chemistry is mostly absent in the circumstellar envelope (CSE) of O-rich stars, most of the carbon being locked up in CO, sulfur chemistry is expected to be relatively active. S-bearing species are indeed commonly observed in the massive CSE around O-rich stars (Sahai & Wannier 1992; Omont et al. 1993).

Under chemical thermodynamical equilibrium, Tsuji (1973) showed that the sulfur in CSEs is mostly

in the form of H₂S. Later non-equilibrium chemical models (Scalo & Slavsky 1980; Nejad & Millar 1988; Willacy & Millar 1997) predict that a large proportion of sulfur should go into SO and SO₂, as a result of the reactions: S + OH → SO + H, HS + O → SO + H and SO + OH → SO₂ + H. OH is a natural product of the photodissociation of H₂O, and VY CMA exhibits intense maser emission for these two species (Bowers et al. 1983; Richards et al. 1998). On the other hand, the production of HS requires highly endothermic reactions. From our SMA observations, the SO and CO morphology and kinematics are similar, implying that SO is present both close to the star and in the bipolar outflow. Observations of Sánchez-Contreras et al. (2000) towards the bipolar nebula OH 231.8+4.2 show a similar trend. These authors argue for the presence of SO both in the central component and in the accelerated lobes, with no significant difference in abundance between the two components.

Assuming optically thin emission and an excitation temperature of $T_{ex} = 40$ K (Sahai & Wannier 1992), we estimate a SO column density $\sim 10^{16}$ cm⁻² towards the center. The corresponding SO abundance relative to H₂ is $\sim 10^{-6}$.

High angular resolution observations of other S-bearing species such as H₂S and SO₂ would provide a better understanding of the sulfur chemistry and put stronger constraints for chemical models.

4. A SIMPLE MODEL OF THE ENVELOPE

We have constructed a simple model in order to better understand the geometry and physical conditions within the circumstellar envelope around VY CMA. The combination of our high angular resolution CO(2-1) data together with previous single dish observations of multiple CO rotational transitions (Kemper et al. 2003) provides very useful constraints for our model and leads us to a coherent picture of the envelope.

The geometry of our model is illustrated in Fig.8. The envelope is assumed to be axisymmetric and radially expanding. The bipolar outflow direction defines the symmetry axis of the envelope. We project the envelope directly into a regular 3-D grid. At each grid point, the gas density, kinetic temperature and expansion velocity can be specified. The emerging CO intensity along each ray through the envelope is calculated by integrating directly the standard radiation transfer equation. We take into account 15 rotational levels of the CO molecule in its vibrational ground state. The populations on the different rotational levels, which are necessary for the calculation of the line opacity and source function at each grid point, are determined by solving the statistical equilibrium equations within the framework of the large velocity gradient formalism. The collision rates between CO and molecular hydrogen are taken from Flower & Launay (1985) and calculated for different temperatures using the prescription of de Jong, Chu & Dalgarno (1975). Because the envelope around VY CMA is oxygen rich, we adopt an abundance $f = [\text{CO}]/[\text{H}_2] = 3 \cdot 10^{-4}$ as used in the analysis of Kemper et al. (2003). The local line profile, which is needed to integrate the radiative transfer equation, is determined through the turbulence velocity of the molecular gas. We assume a turbulence velocity of 1 km s⁻¹ in the slowly expanding envelope and 3 km s⁻¹ in the bipolar lobes, respectively. This assumption is

reasonable as a higher outflow velocity in the lobe would result in more turbulent environment.

As discussed in §3.2.1, two distinct kinematic components are clearly present in the nebula around VY CMA: (1) a slowly expanding envelope slightly elongated in the north-south direction surrounded by a diffuse halo with some extension toward the north-west direction and (2) a high velocity bipolar outflow oriented in the east-west direction. However, to keep our model as simple as possible, we assume that the slowly expanding component is spherically symmetric. We adopt an expansion velocity of 15 km s⁻¹ for this component, which allows us to satisfactorily fit the central peak seen in single-dish CO observations. The presence of diffuse emission suggests that the gas density in the slowly expanding envelope peaks more sharply toward the center than for the case of constant mass loss. We therefore adopt a simple density distribution $n(r) = 4.5 \cdot 10^5 (10^{16} \text{ cm}/r)^{2.5}$, which deviates slightly from the usual density distribution generated by constant mass loss. This adopted distribution corresponds to a mass loss rate $\dot{M} = 4.5 \cdot 10^{-5} (10^{16} \text{ cm}/r)^{0.5} M_{\odot}/\text{yr}$, or a decrease in mass loss rate by a factor of 4 between the inner radius (R_{in}) and the outer radius (R_{out}). The kinetic temperature of the molecular gas in the oxygen-rich circumstellar envelopes with constant mass loss has been known to roughly follow a power law $T(r) \sim r^{-\alpha}$ from the modelling works of Goldreich & Scoville (1976) and Justtanont et al. (1994). Although the mass loss rate in the slowly expanding envelope of VY CMA is not strictly constant, resulting probably in some slight change in the temperature profile in comparison to the simple constant mass loss case, we expect that qualitatively, the temperature profile still follows the power law. Therefore, we assume in our calculations, for the sake of simplicity, that the kinetic temperature varies as $T(r) = 500 \text{ K} (2.25 \cdot 10^{15} \text{ cm}/r)^{0.7}$, which is similar to that used by Kemper et al. (2003) to model the oxygen-rich circumstellar envelopes.

In order to reproduce the velocity gradient seen in the position-velocity diagrams (Fig.6), the outflow velocity in the bipolar lobes is allowed to increase linearly with radial distance from the central star. In addition, the outflow velocity in the bipolar lobes also varies as a function of the polar angle θ measured from the bipolar axis. The strong emission peaks at large velocity shifts suggest the presence of an enhanced density shell within the bipolar lobes. However, this density enhancement is more pronounced in the receding lobe as clearly seen in the position-velocity diagram. With the density enhancement included in the model, we find that the bipolar lobes and the slowly expanding shell can account for the highly unusual triple peak profile of single-dish CO lines observed by Kemper et al. (2003) (see Fig.9).

The intensities of the CO lines calculated along individual lines of sight are used to form the model channel maps (Fig.11). We convolve these model channel maps with a gaussian beam with specified FWHM to produce the model CO line profiles, which are indicated by the dashed lines and compared with the JCMT observations of Kemper et al. (2003) in Fig.9.

We infer from our modelling that the velocity of the gas in the lobes increases linearly from 15 km s⁻¹, which is similar to the expansion velocity of the spherical en-

velope, to 45 km s^{-1} at the outer radius. The bipolar outflow is found to be very open, with an opening angle of 120° , and inclines at 15° from the line of sight. All the model parameters, which provide a reasonable fit to both the SMA and single dish data, are shown in Table 3.

Although relatively simple, our model provides a qualitative understanding of the single dish data obtained by Kemper et al. (2003) and also of the structure of the envelope (Figs.9, 11, 12). The high angular resolution SMA data show that the CO(2-1) emission originating from the high velocity bipolar lobes produces a double horn profile at roughly $\pm 20 \text{ km s}^{-1}$ from the systemic velocity. The central broad peak of the CO(2-1) line comes from the slow component. Higher transitions of CO probe progressively warmer and denser gas located in the inner part of the envelope. However, both the density and temperature of the gas in the inner region of the bipolar outflow, as suggested by our model, are lower than that in the slowly expanding envelope. As a result, the central peak becomes more prominent in higher transitions while the strength of the emission from the bipolar lobes decreases noticeably. In addition, the lower outflow velocity in the inner part of the bipolar lobes also leads to a narrower full width at zero velocity for higher transitions of CO. This behavior can be clearly seen in Fig.9.

By comparing the model prediction for the strength of the $^{13}\text{CO}(2-1)$ line with our SMA observations, we estimate the isotopic ratio $^{12}\text{C}/^{13}\text{C} = 60$. This ratio is significantly larger than the values $^{12}\text{C}/^{13}\text{C} = 6$ and 12 found in the red supergiants α Ori and α Sco, respectively (Harris & Lambert 1984; Hinkle et al. 1976). It is likely that, prior to the current mass loss episode, VY CMa experienced no significant mixing of H burning products to the surface. Our model predicts that most of the $^{13}\text{CO}(2-1)$ line emission should arise from the bipolar outflow (Fig.10), which is consistent with our SMA imaging data (Fig.3).

We emphasize here that our model is constructed to explain the general features of the high resolution SMA data and single-dish CO observations. Other features such as the slight elongation of the slowly expanding shell and the more complicated structure within the bipolar lobes are not considered. However, our model could serve as a useful starting point when higher angular resolution data of CO(2-1) and higher transitions become available in the future.

5. DISCUSSION

5.1. Connection with optical imaging/spectroscopy data

Our high angular resolution CO(2-1) data bring a clearer overall picture of the molecular envelope around the enigmatic red supergiant VY CMa. The envelope consists of two kinematic components: a slowly expanding shell slightly elongated in the north-south direction and a high velocity bipolar outflow oriented in the east-west direction with small inclination angle to the line of sight. The presence of these two kinematic components have already been hinted in previous observations of H_2O and OH masers (Bowers et al. 1983, 1993; Richards et al. 1998). Given the small inclination angle $\sim 15^\circ$ of the bipolar outflows to the line of sight, as derived from our

model and assuming uniform illumination in the nebula, one would expect that the envelope appears only slightly asymmetric with a brighter east lobe (nearer side). However, optical and near IR images obtained by Monnier et al. (1999) and Smith et al. (2001) all show a highly irregular and asymmetric nebula around VY CMa. The nebula is seen to the west and southwest of the bright point-like source identified as the obscured central star VY CMa and is likely the result of a non-isotropic illumination by the central star. Comparing the optical images with our SMA data, we note that the optical nebulosity corresponds to the location of the west (far side) lobe and just a small part of the east (near side) lobe. It is therefore likely that the light from VY CMa escapes preferentially in the direction of the west bipolar lobe and scattering on dust brings a fraction of the light back toward the observer.

The strong 1.3 mm continuum emission detected in our data (see §3.1) confirms the presence of a thick inner dust shell surrounding VY CMa. The average optical depth would be so high, if the distribution of material in the dust shell is smooth, that all the stellar light would be completely extinguished. The complex nebula seen in the optical and near IR then suggests that stellar light must be able to escape through some opening or holes in the dust shell, creating search light beams that illuminate the nebula in an irregular pattern. We note that a similar suggestion was made by Wallerstein (1978) to explain the subtle but peculiar change in the relative position between the star and the brightest knot in the nebula.

The thick and compact inner dust shell detected in 1.3 mm continuum emission might be the region where TiO and ScO bands (Herbig 1974; Wallerstein 1986) seen in emission originate. The calculated excitation temperatures of these molecular bands range from 600 to 800 K, suggesting that they come from a hot and dense region located close to the star.

High resolution optical and near IR images of Monnier et al. (1999) and Smith et al. (2001) show a very prominent long curved tail or arc to the northwest of VY CMa together with several fainter arcs and condensations in the envelope. The location of the long northwest arc roughly coincides with the extended and somewhat diffuse CO(2-1) emission in the western part of the envelope (Fig.2). Together with strong central emission core, this extended emission is conspicuous in all channel maps redshifted with respect to the central star, most prominent in the velocity range $21 - 33 \text{ km s}^{-1}$ and $46 - 54 \text{ km s}^{-1}$. The orientation of this feature changes from west to north-west with increasing velocity upon closer inspection. We can identify a similar feature in the channel maps of the SO emission at the same velocity, although there are some slight differences at higher redshifted velocities, which are probably related to local excitation of the SO molecule. It is therefore possible that the scattering of stellar light by dust in this structure produces the prominent northwest arc seen in optical and near IR images. Future observations of molecular lines at higher angular resolution and detailed modelling of the light scattering by dust inside the envelope will help to clarify the relation between the material distribution and the optical and near IR appearance of the nebula.

Recently, Humphreys et al. (2005) have obtained high

resolution long slit spectroscopic data of VY CMa. By measuring the velocity of the reflected stellar absorption lines and K I emission lines they suggest that the prominent northwest arc is expanding at a velocity of $\sim 50 \text{ km s}^{-1}$ on the plane of the sky. More surprising is the existence of diffuse gas and dust more or less stationary with respect to the central star, mostly along the slit positioned to the southeast of VY CMa (slit V in their Fig.1). Thus, components with very different kinematics seem to co-exist in the nebula. To reconcile the optical spectroscopic data with our SMA results, we note that for the simple case of single scattering, the light scattered by moving reflective material (dust particles) within the envelope is Doppler shifted by $V_{\text{exp}}(1 - \cos\omega)$, where V_{exp} is the expansion velocity and ω is the angle measured from the line of sight to the radial vector of the scattering point (see Fig.8). The velocity shift can be seen to be largest in the west lobe, which is receding along the line of sight, because $\omega > 90^\circ$. If the association of the extended feature in the west lobe as traced by CO emission and the northwest arc is correct, we would expect the velocity shift induced by scattering of moving dust to vary from 15 km s^{-1} for material in the arc moving close to the plane of the sky, which is part of the slowly expanding shell, to $\sim 50 \text{ km s}^{-1}$ or higher for material within the bipolar lobe. This simple estimate of the velocity shift is consistent with the measurement of Humphreys et al. (2005). For absorption lines seen in scattering through the east lobe, the velocity shift is expected to be close to zero because the angle ω is small. That might explain the presence of dust and gas almost stationary with respect to the star as suggested by Humphreys et al. (2005). However, similar behavior seen in resonant K I lines are still difficult to understand.

5.2. Mass loss history

There are strong evidences that the mass loss rate in VY CMa is time variable, such as the prominent arc-like features seen in optical (Smith et al. 2001) and the relative strength of the CO rotational line profiles (Decin et al. 2006).

Our modelling results suggest that the mass loss is varying as $\sim 4.5 \cdot 10^{-5} (10^{16} \text{ cm}/r)^{0.5} M_{\odot}/\text{yr}$ in the slowly expanding envelope ($V_{\text{exp}} = 15 \text{ km s}^{-1}$), *i.e.* that the mass loss from VY CMa is increasing with time, reaching $\sim 6.4 \cdot 10^{-5} M_{\odot}/\text{yr}$ in the inner part of the envelope (R_{in}) or about 100 years ago. In the bipolar lobes, the density enhancement between $5 - 7 \cdot 10^{16} \text{ cm}$ represents an episode of strong mass loss about 350 to 500 years ago, for the expansion velocity of 45 km s^{-1} . The nominal mass loss rate at $6 \cdot 10^{16} \text{ cm}$ is $10^{-3} M_{\odot}/\text{yr}$. A similar episode of intense mass loss has also been inferred from modelling results of Decin et al. (2006), although their assumption of spherical symmetry is inadequate to describe the geometry and kinematics of the nebula around VY CMa.

The current mass loss from VY CMa is better traced by dust continuum emission in the mid infrared or millimeter and sub-millimeter wavelengths. We derived a mass loss rate of $4.7 \cdot 10^{-4} M_{\odot}/\text{yr}$ from 1.3 mm dust continuum emission. This value is very close to that obtained by Harwit et al. (2001) from fitting infrared spectroscopic data. As already noted by Decin et al. (2006), the difference between mass loss rate derived from CO line profiles and dust continuum suggests that the dust continuum

emission originates from the inner dense and hot region (a few tens of stellar radii from the central star), which is not well traced by CO low rotational lines.

5.3. Origin of the complex envelope around VY CMa

The origin of the bipolar outflow and the north-south elongated structure in VY CMa is still unclear at present. However, we note the similarity in morphology (bipolar outflows and/or disk-like structures) between the envelope of VY CMa and that around several AGB and post-AGB stars such as π^1 Gru (Chiu et al. 2006), V Hya (Hirano et al. 2004), M 2-56 (Castro-Carrizo et al. 2001) and X Her (Nakashima 2005). The current popular model proposed by Morris (1987) to explain the striking bipolar morphology and the presence of collimated fast outflow in AGB and post-AGB envelopes involves a low mass binary companion. The companion can have strong effect on the structure of the envelope. Its gravitational pull can focus the AGB wind toward the orbital plane to create an equatorial density enhancement. In addition, the accretion of wind material into the companion leads to the formation of an accretion disk, which might drive the collimated high velocity outflow. Although the overall morphology of the envelope is similar to that around other AGB and post-AGB stars, the high velocity wind from VY CMa, as suggested by our data and modelling results, is only weakly collimated with very wide opening angle. It is conceivable that the interaction between an unseen companion and VY CMa could produce equatorial density enhancement, possibly identified as the elongated structure and induce the collimated fast wind to precess. Subsequent interaction with the nebula would result in wide bipolar lobe. The prominent curved nebulous tail seen in scattered light and the extended and curved structure seen in our CO(2-1) data might actually trace the precessing outflow. To explain the prominent nebulous tail, Monnier et al. (1999) also suggest the existence of a rotating jet and estimate the rotation period of a few thousands years. That time scale might be related to the orbital period of an unseen companion around VY CMa. However, high resolution images from Smith et al. (2001) suggest that this structure is actually much more complicated than expected from the model of Monnier et al. (1999) and probably more consistent with a localized ejection event on the stellar surface. Our current SMA data cannot distinguish between these possibilities. Future high angular resolution observations and monitoring are necessary to determine the distribution of material and kinematics in order to test the presence of a companion.

VY CMa might have magnetic activity, resembling solar flares or eruptions, as suggested by Smith et al. (2001) in order to explain the presence of numerous arcs and bright knots seen in scattered light in the nebula. We speculate further that the bipolar flow with wide opening angle and the equatorial density enhancement could be similar to what is observed in the solar wind. The fast solar wind originates from coronal holes located near the poles where magnetic field lines are open and the slower but denser wind comes from the equatorial region. The geometry of the solar wind is closely coupled to the dipolar field of the Sun. In the case of VY CMa, the presence and strength of the magnetic field can only be inferred indirectly from observations of SiO, H₂O and

OH masers. Observations of Zeeman effect in SiO maser lines suggest a strength of 0 – 2 G (Herpin et al. 2006) for the magnetic field around VY CMa. Using simple estimates, Soker (1998) and Soker & Zoabi (2002) suggest that a magnetic field of about 1 G can significantly influence the outflow. The observed strength of the magnetic field in VY CMa thus suggests that it might affect the dynamics of the wind and if the field is organised on large scale, *i.e.* dipolar configuration, it could explain the structure of the envelope as seen in our SMA data.

6. CONCLUSION

In this paper, we present high angular resolution observations of the circumstellar molecular envelope of the red supergiant VY CMa obtained with the Submillimeter Array. Thanks to the wide frequency coverage of the SMA, we were able to trace the envelope in the $^{12}\text{CO}(2-1)$, $^{13}\text{CO}(2-1)$ and $\text{SO}(6_5-5_4)$ lines and dust continuum emission. We detected a strong and unresolved continuum emission at the center of the nebula. The derived dust mass is $1.5 \cdot 10^{-3} M_{\odot}$, implying a lower limit of the recent mass loss of $4.7 \cdot 10^{-4} M_{\odot}/\text{yr}$ over the last 300 years. The $\text{CO}(2-1)$ emission is resolved into two distinct kinematic components: a slowly (15 km s^{-1}) expanding shell elongated in the north-south direction and a high velocity (45 km s^{-1}) component with a clear velocity gradient along the east-west direction. Similar structures

are also seen in the $^{13}\text{CO}(2-1)$ and $\text{SO}(6_5-5_4)$ emission. We interpret the high velocity component as a bipolar outflow with a wide opening angle ($\sim 120^\circ$), for which the symmetry axis is oriented close to the line of sight ($i = 15^\circ$). Using a simple model, we could explain the main features of the $\text{CO}(2-1)$ emission in our SMA data as well as the previous single-dish CO multi-line observations. Density enhancement in the outflows, representing a previous episode of high mass loss, is inferred from our model. Our data complement previous high resolution optical spectroscopy and optical/IR images and provide a better understanding of the complicated morphology of the nebula around VY CMa. Future high resolution and high sensitivity observations of CO lines, including high-J transitions, will allow us to study the structure of the envelope and its physical properties in more detail.

We are very grateful to F. Markwick-Kemper for providing us her JCMT CO spectra on VY CMa. This work is supported in part by Academia Sinica and by grants from the National Science Council of Taiwan (NSC) to D.-V.-T. (NSC 94-2112-M-001-008), J.L., and S.K. This research made use of NASA's Astrophysics Data System, as well as the SIMBAD database operated at CDS, Strasbourg, France.

REFERENCES

- Bowers, P. F., Johnston, K. J. & Spencer, J. H., 1983, *ApJ*, 274, 733
 Bowers, P. F., Claussen, M. J. & Johnston, K. J., 1993, *AJ*, 105, 284
 Castro-Carrizo, A., Lucas, R., Bujarrabal, V., Colomer, F. & Alcolea, J., 2001, *A&A*, 368, L34
 Chiu, P.-J., Hoang, C.-T., Dinh-V-Trung, et al., 2006, *ApJ*, 645, 605
 Danchi, W. C., Bester, M., Degiacomi, C. G., Greenhill, L. J. & Townes, C. H., 1994, *AJ*, 107, 1469
 Decin, L., Hony, S., de Koter, A., et al., 2006, *A&A*, 456, 549
 de Jong, T., Chu S.-I. & Dalgarno, A., 1975, *ApJ*, 199, 69
 Flower, D. R. & Launay, J. M., 1985, *MNRAS*, 214, 271
 Goldreich, P. & Scoville, N., 1976, *ApJ*, 205, 144
 Harris, M. J. & Lambert, D. L., 1984, *ApJ*, 281, 739
 Harwit, M., Malfait, K., Decin, L., et al., 2001, *ApJ*, 557, 844
 Herbig, G. H., 1970, *ApJ*, 162, 557
 Herbig, G. H., 1974, *ApJ*, 188, 533
 Herpin, F., Baudry, A., Thum, C., Morris, D. & Wiesemeyer, H., 2006, *A&A*, 450, 667
 Hinkle, K. H., Lambert, D. L. & Snell, R. L., 1976, *ApJ*, 210, 684
 Hirano, N., Shinnaga, H.; Dinh-V-Trung, et al., 2004, *ApJ*, 616, L43
 Ho, P. T. P., Moran, J. M. & Lo, K. Y., 2004, *ApJ*, 616, L1
 Humphreys, R. M., Davidson, K., Ruch, G. & Wallerstein, G., 2005, *AJ*, 129, 492
 Justtanont, K., Skinner, C. J. & Tielens, A. G. G. M., 1994, *ApJ*, 435, 852
 Kemper, F., Stark, R., Justtanont, K., et al., 2003, *A&A*, 407, 609
 Knapp, G. R., Sandell, G. & Robson, E. I., 1993, *ApJS*, 88, 173
 Lada, C. J. & Reid, M. J., 1978, *ApJ*, 219, 95
 Lipsky, S. J., Jura, M. & Reid, M. J., 2005, *ApJ*, 626, 439
 Monnier, J. D., Tuthill, P. G., Lopez, B., et al., 1999, *ApJ*, 512, 351
 Morris, M., 1987, *PASP*, 99, 1115
 Nakashima, J., 2005, *ApJ*, 620, 943
 Nejad, L. A. M. & Millar, T. J., 1988, *MNRAS*, 230, 76
 Netzer, N. & Knapp, G. R., 1987, *ApJ*, 323, 734
 Omont, A., Lucas, R., Morris, M. & Guilloteau, S., 1993, *A&A*, 267, 490
 Perryman, M. A. C., Lindergren L., Kovalesky J., et al., 1997, *A&A*, 323, L49
 Richards, A. M. S., Yates, J. A. & Cohen, R. J., 1998, *MNRAS*, 299, 319
 Sahai, R. & Wannier, P. G., 1992, *ApJ*, 394, 320
 Sánchez-Contreras, C., Bujarrabal, V., Neri, R. & Alcolea, J., 2000, *A&A*, 357, 651
 Scalo, J. M. & Slavsky, D. B., 1980, *ApJ*, 239, L73
 Shinnaga, H., Claussen, M. J., Lim, J., Dinh-van-Trung & Tsuboi, M., 2003, in *ASSL Vol. 283, Mass-Losing Pulsating Stars and their Circumstellar Matter*, eds. Nakada, Honma, Y. M. & Seki M. (Dordrecht: Kluwer), 393
 Shinnaga, H., Moran, J. M., Young, K. H. & Ho, P. T. P., 2004, *ApJ*, 616, L47
 Smith, N., 2004, *MNRAS*, 349, L31
 Smith, N., Humphreys, R. M., Davidson, K., et al., 2001, *AJ*, 121, 1111
 Soker, N., 1998, *MNRAS*, 299, 1242
 Soker, N. & Zoabi, E., 2002, *MNRAS*, 329, 204
 Stanek, K. Z., Knapp, G. R., Young, K. & Phillips, T. G., 1995, *ApJS*, 100, 169
 Tsuji, T., 1973, *A&A*, 23, 411
 Wallerstein, G., 1978, *Observatory*, 98, 224
 Wallerstein, G., 1986, *A&A*164, 101
 Walmsley, C. M., Chini, R., Kreysa, E., et al., 1991, *A&A*, 248, 555
 Willacy, K. & Millar, T. J., 1997, *A&A*, 324, 237
 Wittkowski, M., Langer, N. & Weigelt, G., 1998, *A&A*, 340, L39
 Wright, M. C.H., Carlstrom, J. E., Plambeck R. L. & Welch W. J., 1990, *AJ*, 99,1299

Table 1: Basic data of VY CMa

R.A. (J2000)	07 ^h 22 ^m 58 ^s .3315	(1)
Dec. (J2000)	-25°46′03″.174	(1)
Distance	1.5 kpc	(2)
Angular scale	1″ ∼ 1500 AU ∼ 2.25 10 ¹⁶ cm	
Luminosity L _*	∼ 2 10 ⁵ L _⊙	(3)
Effective temperature T _{eff,*}	2800 K	(3)
Stellar radius R _*	1.2 10 ¹⁴ cm	(3)
Stellar mass M _*	≥ 15 M _⊙	
Mass loss rate \dot{M}	∼ 2 - 4 10 ⁻⁴ M _⊙ /yr	(4)

REFERENCES. — (1) from the Hipparcos catalogue, Perryman et al. (1997); (2) Lada & Reid (1978); (3) Monnier et al. (1999); (4) Bowers et al. (1983), Danchi et al. (1994), Stanek et al. (1995), Harwit et al. (2001).

Table 2: SMA line observations towards VY CMa.

Line	Rest freq. (GHz)	Synthesized beam (arcsec)	P.A. (deg.)	Vel. res. (km s ⁻¹)	1σ rms (mJy/beam)
¹² CO(2-1)	230.538	1.94 x 1.67	0	4.2	140
¹³ CO(2-1)	220.399	2.65 x 2.30	147	11	65
SO(6 ₅ -5 ₄)	219.949	1.99 x 1.80	155	4.4	110

Table 3: Parameters of our model

Envelope inner radius (R _{in})	5 10 ¹⁵ cm	
Envelope outer radius (R _{out})	8 10 ¹⁶ cm	
Bipolar lobe inner radius (R _{lobe})	1.5 10 ¹⁶ cm	
Opening angle of the bipolar lobes	120°	
Envelope expansion velocity	15 km s ⁻¹	
Expansion velocity in the bipolar lobes	[30 - 10 tanθ/tan(60°)] (r - R _{lobe})/(R _{out} - R _{lobe}) + 15 km s ⁻¹ †	
Gas density in the envelope	4.5 10 ⁵ (10 ¹⁶ cm/r) ^{2.5} cm ⁻³	
Gas temperature in the envelope	500 (2.25 10 ¹⁵ cm/r) ^{0.7} K	
Gas density in the bipolar lobes	6 10 ⁴ cm ⁻³	for R _{lobe} < r < 5 10 ¹⁶ cm
...	10 ⁵ cm ⁻³	for 5 10 ¹⁶ cm < r < 7 10 ¹⁶ cm
...	10 ⁵ (7 10 ¹⁶ cm/r) ² (cm ⁻³)	for r > 7 10 ¹⁶ cm
Gas temperature in the bipolar lobes	150 (1.5 10 ¹⁶ cm/r) ^{0.7} K	for R _{lobe} < r < 5 10 ¹⁶ cm
...	35 K	for 5 10 ¹⁶ cm < r < 7 10 ¹⁶ cm
...	35 (7 10 ¹⁶ cm/r) K	for r > 7 10 ¹⁶ cm
Inclination angle	15°	
Position angle of the nebula axis	90°	
f=[CO]/[H ₂]	3 10 ⁻⁴	
¹² C/ ¹³ C	60	
Total molecular gas mass in the envelope	0.15 M _⊙	

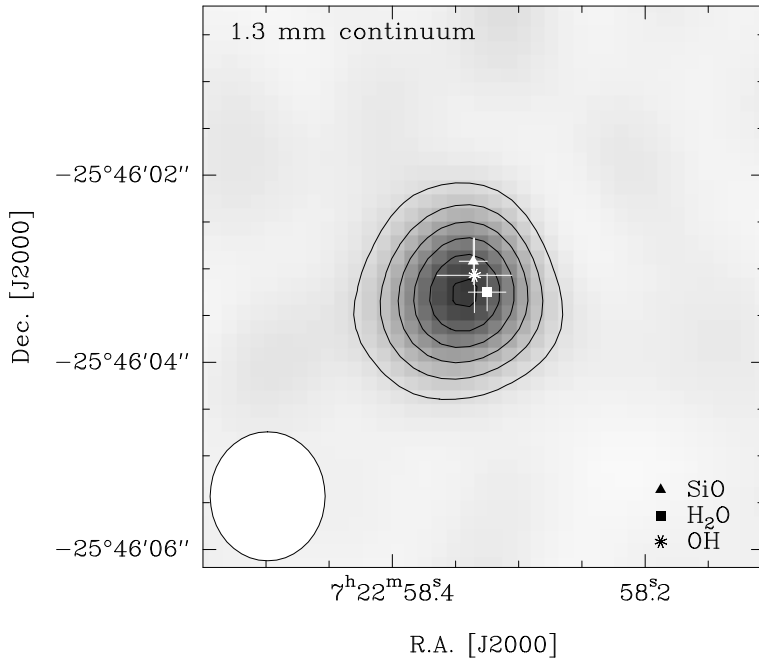


FIG. 1.— 1.3 mm continuum emission map of VY CMa. The synthesized beam is $1.38'' \times 1.23''$ ($PA = 169^\circ$) as indicated by the ellipse in the bottom left corner. Contour levels are every 40 mJy/beam (5σ). The positions of the SiO (Wright et al. 1990), H₂O (Bowers et al. 1993) and OH (Bowers et al. 1983) maser centroids are indicated. The 1.3 mm continuum peak is located at R.A. = $07^{\text{h}}22^{\text{m}}58^{\text{s}}.339$ and Dec. = $-25^\circ46'03''.24$ (J2000).

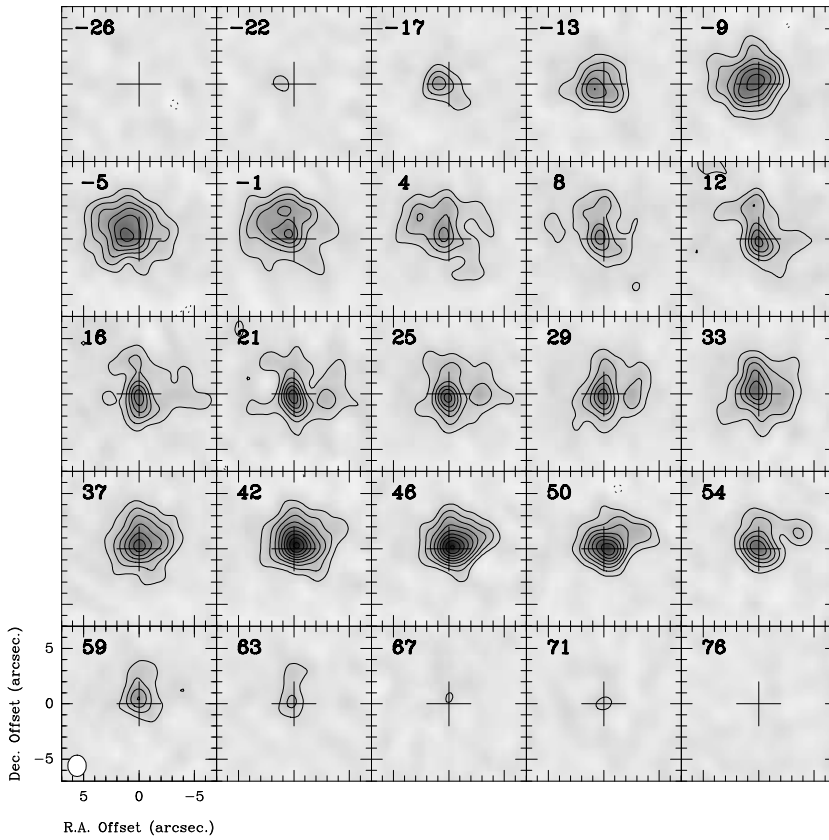


FIG. 2.— Channel maps of the $^{12}\text{CO}(2-1)$ line emission. The synthesized beam sizes $1.94'' \times 1.67''$ ($PA = 0^\circ$) and is shown in the bottom left corner of the figure. Contour levels are drawn every 0.55 Jy/beam or 3.9 K ($\sim 4\sigma$). The velocity resolution is 4.2 km s^{-1} . The cross indicates the position of the phase center.

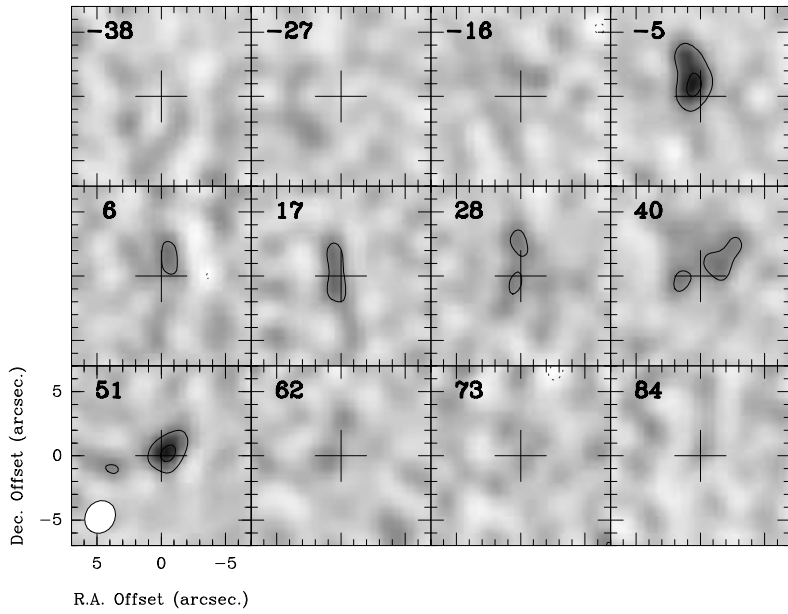


FIG. 3.— Channel maps of the $^{13}\text{CO}(2-1)$ line emission. The synthesized beam sizes $2.65'' \times 2.30''$ (PA = 147°) and is shown in the bottom left corner of the figure. Contour levels are drawn every 0.2 Jy/beam or 0.82 K ($\sim 3\sigma$). The velocity resolution is 11 km s^{-1} . The cross indicates the position of the phase center.

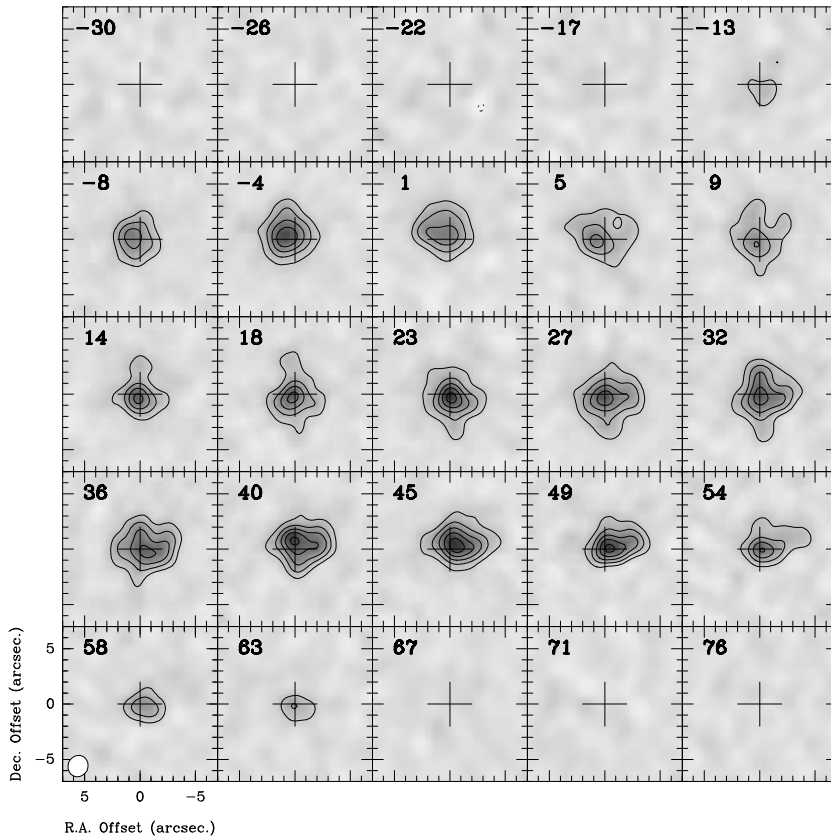


FIG. 4.— Channel maps of the $\text{SO}(6_5-5_4)$ line emission. The synthesized beam sizes $1.99'' \times 1.80''$ (PA = 155°) and is shown in the bottom left corner of the figure. Contour levels are drawn every 0.44 Jy/beam or 3.1 K ($\sim 4\sigma$). The velocity resolution is 4.4 km s^{-1} . The cross indicates the position of the phase center.

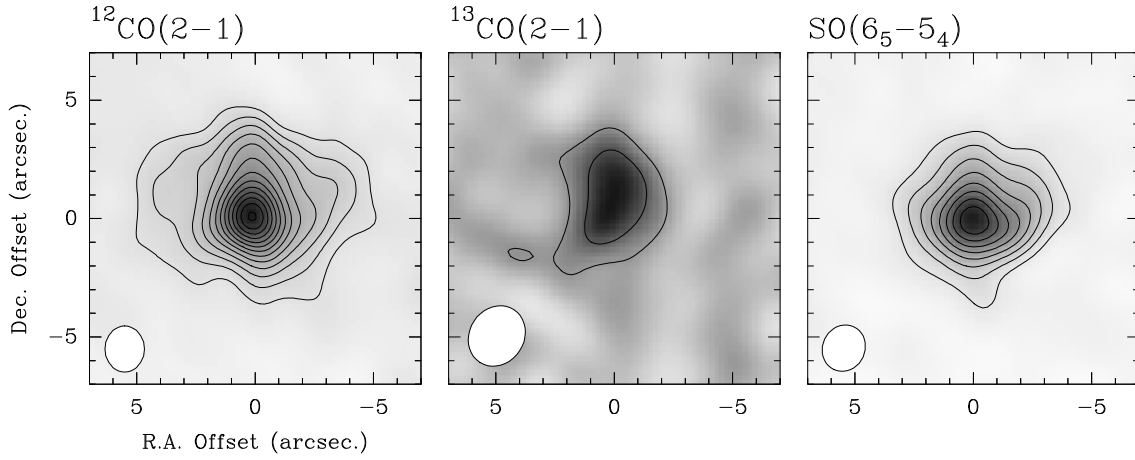


FIG. 5.— Integrated maps of the $^{12}\text{CO}(2-1)$, $^{13}\text{CO}(2-1)$, $\text{SO}(6_5-5_4)$ emission lines. The synthesized beam sizes are indicated in the bottom left corner of each frame. Contour levels are every 140 (7σ), 30 (3σ), and 105 (7σ) K km s^{-1} respectively. Offsets refer to the position of the phase center.

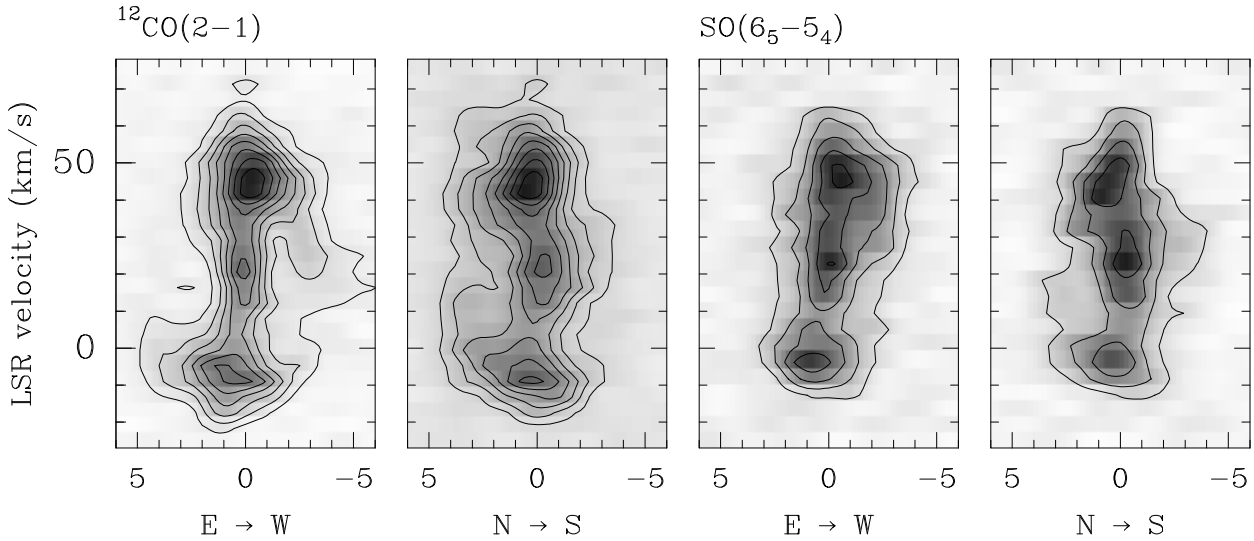


FIG. 6.— Position - velocity diagrams along the east-west and north-south directions for the $^{12}\text{CO}(2-1)$ and $\text{SO}(6_5-5_4)$ line emissions. Countour levels every 0.60 and 0.48 Jy/beam (4σ), respectively.

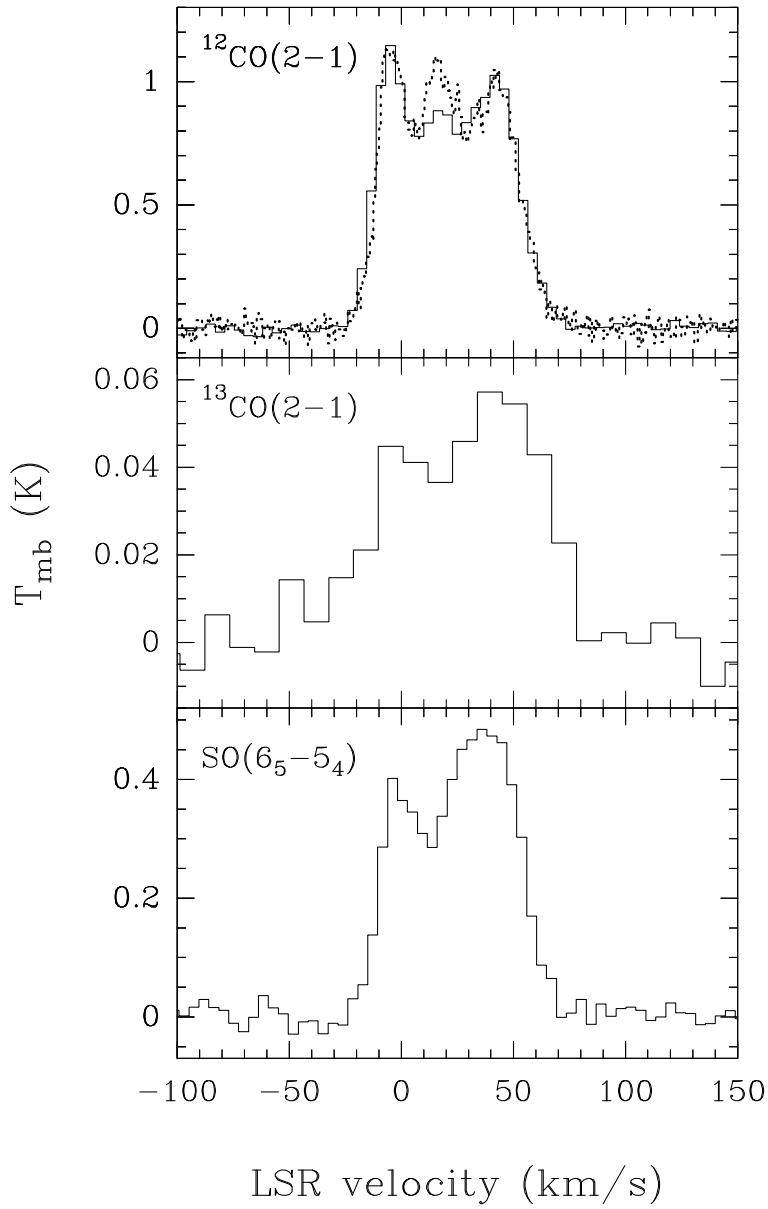


FIG. 7.— Spectra of the $^{12}\text{CO}(2-1)$, $^{13}\text{CO}(2-1)$ and $\text{SO}(6_5-5_4)$ lines smoothed to a $19''.7$ FWHM beam. The $^{12}\text{CO}(2-1)$ spectrum observed with the JCMT by Kemper et al. (2003) is shown as a dashed line in the upper panel. The velocity resolution is 4.2, 11 and 4.4 km s^{-1} from top to bottom.

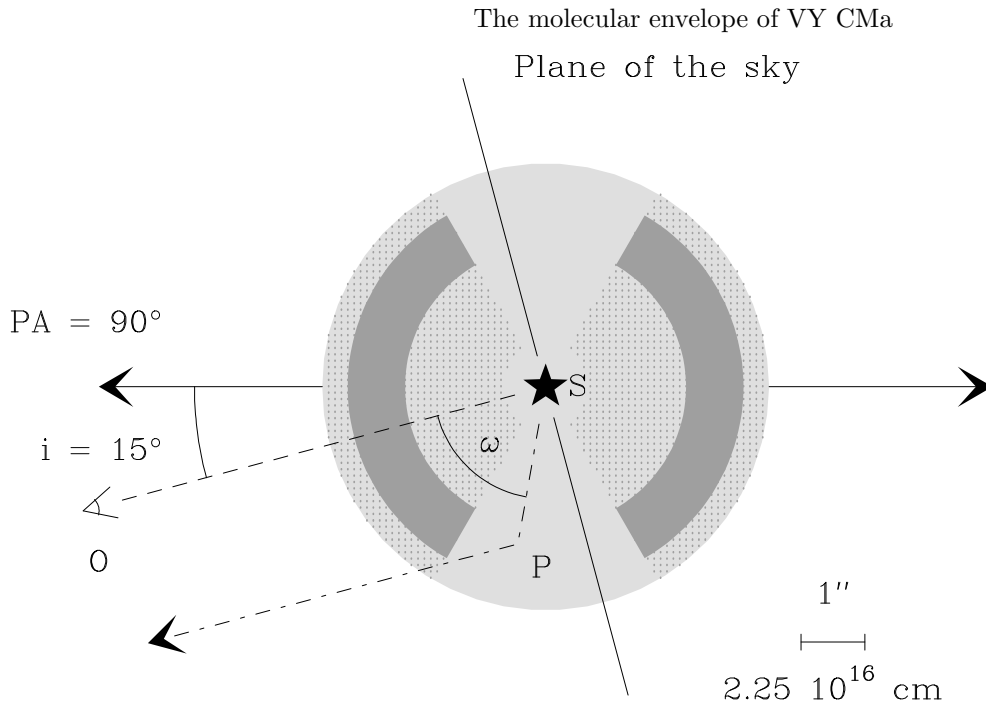


FIG. 8.— Sketch of the geometry of our model. The central star VY CMa (S) is embedded in a spherically symmetric slowly expanding envelope (light grey). Part of the nebula is occupied by a bipolar outflow with a wide opening angle (dotted pattern). Regions of density enhancement within the bipolar lobes are also included (filled bands). The line of sight OS intercepts the bipolar outflow axis with an inclination angle of 15° . A stellar photon is scattered at point P inside the envelope to the observer. The angle ω is defined as \widehat{OSP} .

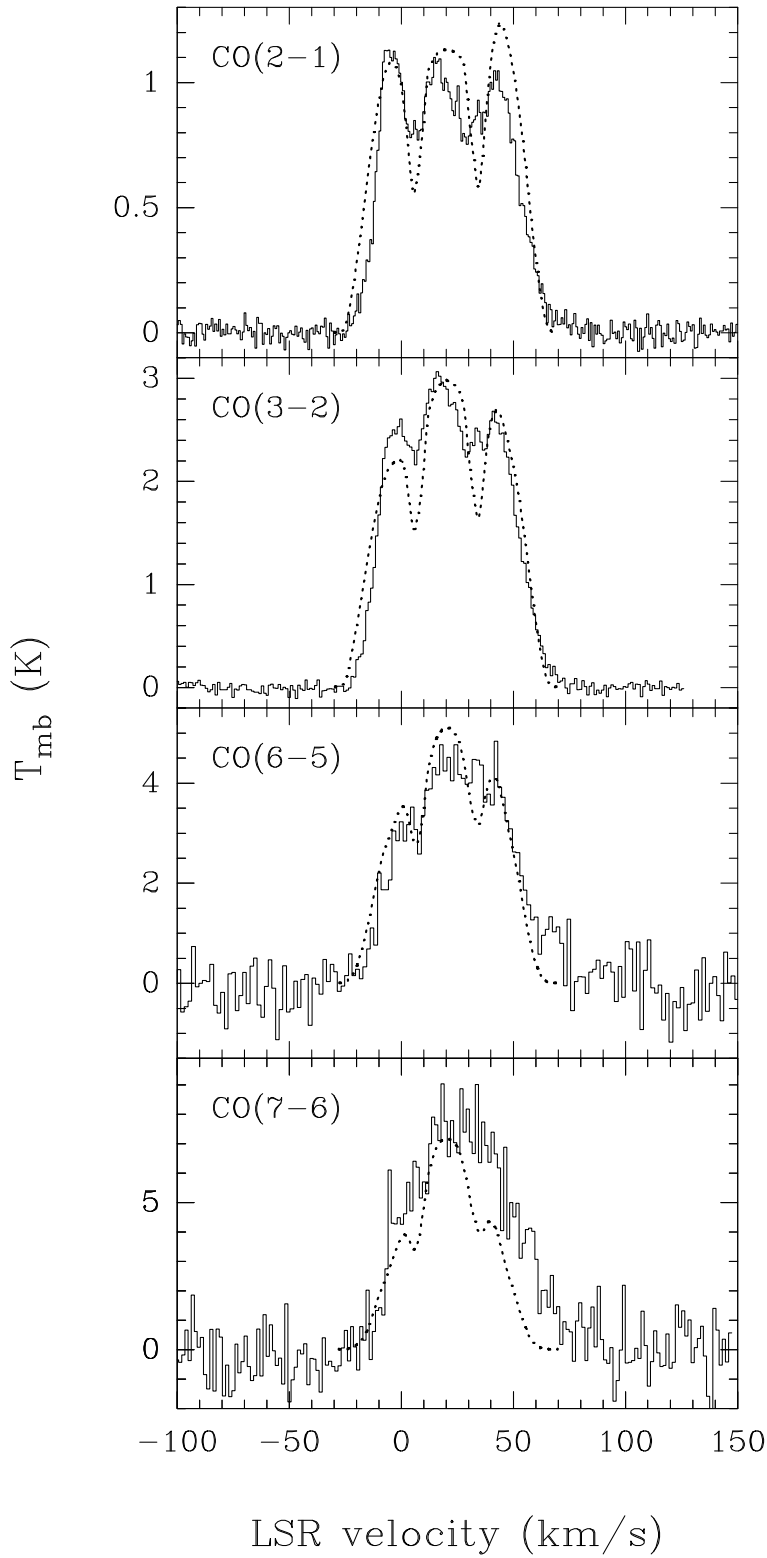


FIG. 9.— Spectra of the CO(2-1), CO(3-2), CO(6-5) and CO(7-6) lines observed by Kemper et al. (2003) using JCMT are shown (full lines) together with the predicted CO line profiles from our model (dotted lines).

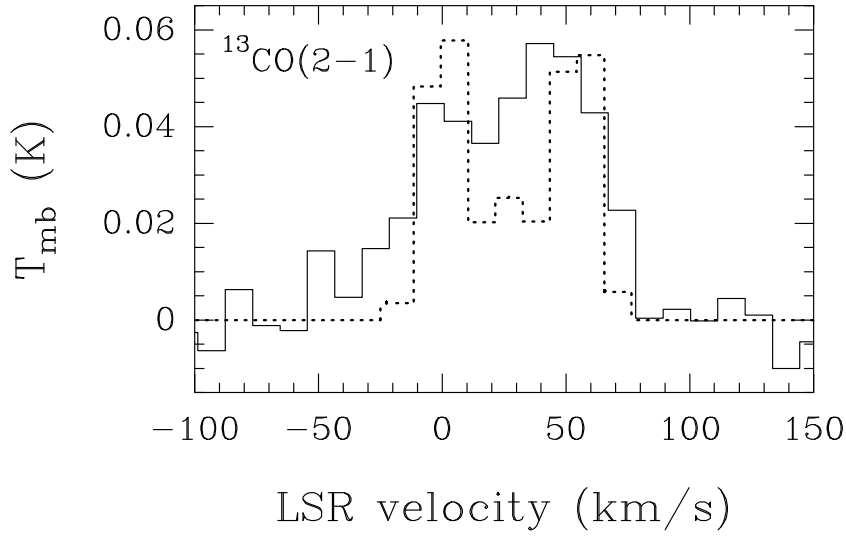


FIG. 10.— SMA spectrum of the $^{13}\text{CO}(2-1)$ line convolved with a $19''.7$ FWHM beam (full line) together with the output spectrum from our model (dotted line). The model spectrum is smoothed to the same velocity resolution of the SMA data (11 km s^{-1}). A ratio $^{12}\text{C}/^{13}\text{C} = 60$ was inferred from our modelling.

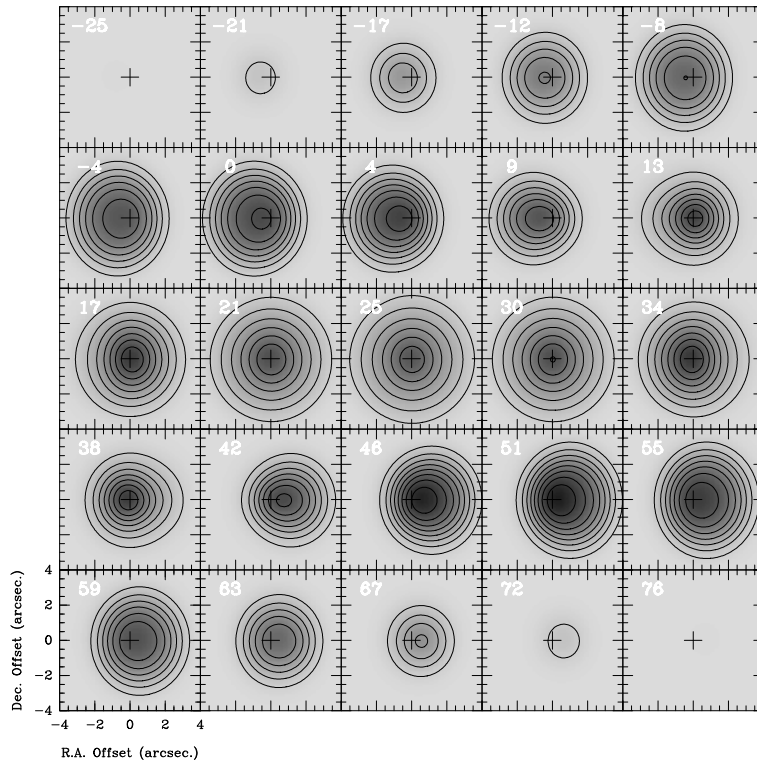


FIG. 11.— Predicted channel maps of the $\text{CO}(2-1)$ emission from the envelope around VY CMa. Contour levels are the same as in Fig. 2.

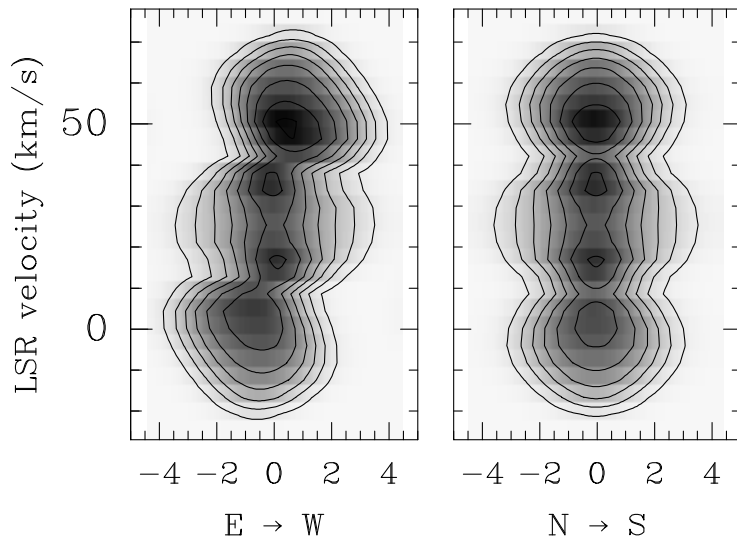


FIG. 12.— Predicted position-velocity diagram of the CO(2-1) emission along the east-west (left frame) and north-south (right frame) direction.